OPTOELECTRONICS AND ADVANCED MATERIALS – RAPID COMMUNICATIONS Vol. 3, No. 9, September 2009, p. 891 - 898

Photo-physical properties of of ZnS/PVA nanocrystals

J. P. BORAH*, K. C. SARMA
Department of Instrumentation and USIC , Gauhati University, Guwahati 781014, India

Polyvinyl-alcohol (PVA) has been used as the matrix to synthesize ZnS /PVA composite films by means of the Chemical method. The as-obtained films were characterized by X-ray diffraction (XRD), Transmission electron microscopy (TEM), Atomic force microscopy (AFM), Ultraviolet–visible (UV–VIS) absorption, and photoluminescence (PL) spectra. The results confirmed that the size of the as-synthesized ZnS nanoparticles depends on the amount of $ZnCl_2$ salt. The photoluminescence and UV–VIS spectroscopy revealed that the ZnS/PVA films showed quantum confinement effect. The primary FTIR spectra of ZnS/PVA nanocomposite in different PVA:$ZnCl_2$ have been discussed. The results indicate that the introduction of ZnS decreased the degree of crystallinity of PVA.

(Received July 09, 2009; accepted September 15, 2009)

Keywords: II–VI semiconductors, Nanocrystalline materials, Optical properties

1. Introduction

Nanoparticles are of great interest due to their extremely small size and large surface-to-volume ratio, which lead to both chemical and physical differences in their properties, compared to bulk of the same chemical composition. The physical properties of semiconductor nanocrystallites are dominated by the spatial confinement of excitations (electronic and vibrational). Quantum confinement, the widening HOMO LUMO gap with decreasing crystallite size, and its implications for the electronic structure and photophysics of the crystallites have generated considerable interest. The semiconductor nanoparticles may find applications in nonlinear optical devices, photocatalysis, etc. [1–3]. Semiconductor nanocrystals in a transparent matrix, particularly based on polymers, have recently attracted interest due to their potential in applications in nonlinear optics such as photonic switching [4] and [5]. The polymer matrix has several important roles to play. It provides the confinement potential in view of its larger band-gap relative to the semiconductor material. It also hosts the nanocrystal in the form of a stable matrix. As a transparent host, it can also render the nanocrystals in a form suitable for applications in linear and nonlinear optics. Various polymers [6-10] have been used as host matrices for embedding semiconductor nanocrystals. ZnS, an important member of group II–VI semiconductor phosphor with wide band gap energy of 3.7 eV, has attracted much research interest due to its potential applications in optoelectronic devices such as solar cells and infrared windows. ZnS on account of being a versatile and excellent phosphor material shows a variety of luminescence properties that enable it to have applications in the fields of flat displays, sensors, and lasers [11–14]. In addition, ZnS behaves as an effective catalyst and has attracted the attention in the fields of photosynthesis and pollutant treatment [15–17]. Polyvinyl alcohol (PVA) is a hydrophilic polymer frequently used as a matrix for stabilization of ZnS nanocrystals extensively [18], [19]. PVA does not allow much scope for size tunability of ZnS nanocrystals at room temperature due to the interaction between polymer and inorganic phase.

In this article we report the synthesis of polymer-capped nanocrystalline ZnS thin films by a chemical synthesis process. We have studied the changes of structural, optical and morphological properties of these films with the variation of molecular content of the film.

2. Experimental studies

2.1 Preparation of ZnS-PVA nanocomposites

ZnS nanoparticle are synthesized in the polymer matrix by an ion exchange reaction. A typical synthesis is carried out as follows: 5 wt% solution of PVA, $ZnCl_2$ were mixed with various concentration (1,2,3,4 wt%) under a high stirring rate (200rpm) condition. The constant temperature 70^0C for 3 hours was maintained during the process of stirring. The sample under preparation was kept for 12 hours for complete dissolution to get a transparent solution. To this solution 2 wt% Na_2S was added till the whole solution turns into milky The ZnS nanoparticle

containing PVA were caste over glass slides to produce thin film form and successive experiments for characterization were carried out. The chemical reaction occurs as follows

$$ZnCl_2+Na_2S \longrightarrow ZnS +2NaCl$$

2.2 Characterization of ZnS-PVA nanocomposites

X-ray powder diffractograms (XRD) of the samples are taken on a Philips X'Pert Pro diffractometer operating at 40KV-30mA The radiation source used was CuKα (λ =1.542Å) and a Nickel filter was used to block K_{β} Radiations. The diffractograms of the samples are recorded in the step-scanning geometry, with a step width of 0.02° and 10 s count time so as to improve the signal-to-noise ratio. XRD of polyvinyl alcohol is taken in the continuous scan mode for the purpose of comparison.

Optical absorption spectra of the samples are recorded using (HITACHI-U3210) double beam spectrophotometer in the range 200-800 nm, at a wavelength resolution of 0.1 nm. The spectra are corrected for the base line. Photoluminescence spectra are recorded on a Thermospectronic AMINCO Bowman (series2) fluorescence spectrometer. The emission spectra are recorded for different excitation energies greater than the band gap of the samples. Excitation spectra corresponding to the two emission bands observed in photoluminescence emission are also recorded. All the spectra are corrected for the instrumental spectral response. The PERKIN ELMER Fourier transform infrared spectroscope (FTIR) was employed to monitor the formation process of ZnS/PVA nanocomposites films.

TEM observations of the ZnS nanocrystals are performed by using (model JEOL JEM-100cx) transmission electron microscope, operating at 400 kV accelerating voltage. The surface morphology and surface roughness of the films was determined by AFM. The AFM measurements were performed in contact mode in air by using a molecular imaging microscope (model PICO Scan 2500). The cantilever force constant 0.21 N/m were used.

3. Results and discussion

Fig. 1 shows the XRD pattern of four different ZnS nanocrystalline film under optimum growth conditions but at different PVA:$ZnCl_2$ ratio 5:1,5:2,5:3 and 5:4. The optimum pH value for minimum size was fixed at 1.7. All the spectra included peaks at 2θ = 19.6^0, which corresponded to the crystalline phase of PVA [20]. The other peaks with 2θ values of 28.6, 47.8 and 56.6 corresponded to the (111), (220), (311) crystalline planes of ZnS and these peaks could be indexed to Cubic ZnS with lattice constants of a = 5.406 A °, which were consistent with the literature data of JCPDS 5-0566. It is known that the crystalline nature of PVA results from the strong intermolecular interaction between PVA chains through the intermolecular hydrogen bonding [21].

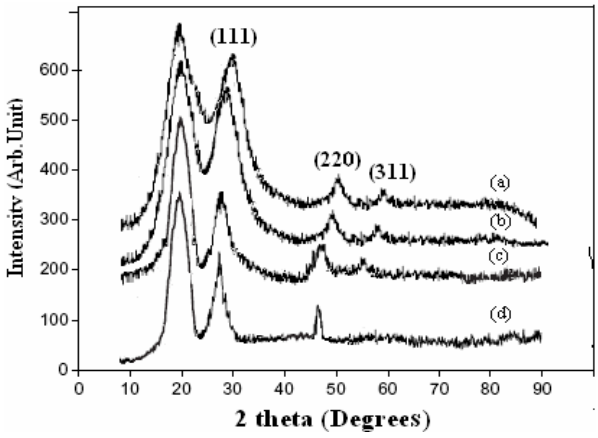

Fig. 1 XRD patterns of the PVA films containing ZnS nanoparticles, prepared at different PVA:$ZnCl_2$ ratio (a) 5:1 (b) 5:2(c) 5:3 (d) 5:4.

It is seen in Fig. 1 that PVA lines were weaken with the increasing amount of $ZnCl_2$ salt. It should be the reason that the interactions between PVA chains and ZnS particles led to the decrease of intermolecular interaction of PVA chains, which would result in decreasing the crystalline degree of PVA. The systematic errors in 2θ were eliminated by applying the function determined by Nelson and Riley in ZnS films from three prominent reflections. The corrected value of lattice constant 'a' is then obtained by extrapolating the function F(θ) to zero[22]. Where

$$F(\theta) = \frac{1}{2}\left(\frac{Cos^2\theta}{Sin\theta} + \frac{Cos^2\theta}{\theta}\right) \quad (1)$$

The diffraction peaks of ZnS nanoparticle at different PVA: $ZnCl_2$ ratio can be indexed as face centered cubic phase and the lattice constants are calculated as a=5.367 Å, being close to the reported values (a=5.406 Å, JCPDS 5-0566). Putting a_{cal} values against extrapolating function F (θ) we get the Nelson Riley plot as shown in Fig. 2.

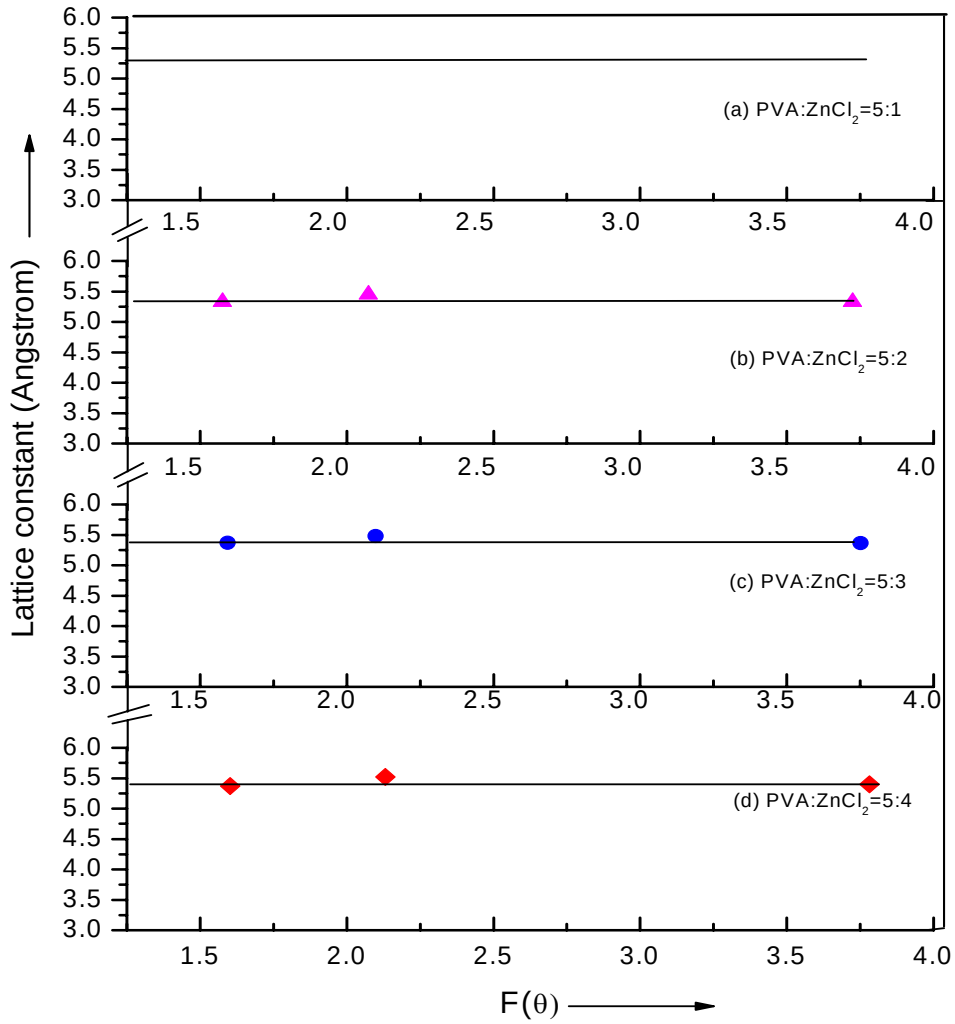

Fig. 2. Nelson Riley plot for ZnS nanoparticles, prepared at different amount of PVA: $ZnCl_2$ ratio (a) 5:1 (b) 5:2 (c) 5:3(d) 5:4.

Table 1. Values of lattice constant determined from Nelson Riley plot at different PVA: $ZnCl_2$ values.

Sample No.	PVA:$ZnCl_2$	hkl	d value (Å)	2θ (degree)	F (θ)	a_{cal} (Å)	Nelson Riley plot (Å)
(a)	5:4	111	3.121	28.6	3.7819	5.40	5.39
		220	1.967	46.14	2.1311	5.55	
		311	1.622	56.6	1.6022	5.37	
(b)	5:3	111	3.098	28.8	3.7522	5.36	5.37
		220	1.9413	46.7	2.0975	5.48	
		311	1.619	56.8	1.5939	5.37	
(c)	5:2	111	3.075	29	3.724	5.32	5.35
		220	1.927	47.1	2.074	5.45	
		311	1.607	57.2	1.577	5.33	
(d)	5:1	111	3.034	29.4	3.729	5.25	5.303
		220	1.898	47.8	2.033	5.37	
		311	1.601	57.5	1.564	5.31	

The values of lattice constant and d spacing at different reagent concentration are shown in Table 1 It is seen that as the amount of $ZnCl_2$ concentration decreases the lattice constant decreases i.e. Increase in diffraction angle is clearly a result of lattice contraction expected to occur because of higher surface to volume ratio [23-24].

The average size (L) of the ZnS nanocrystallites and the lattice strain (ε) of these films were calculated using the equation 2 given by Williamson & Hall [25].

$$\frac{\beta Cos\theta}{\lambda} = \frac{\varepsilon Sin\theta}{\lambda} + \frac{1}{L} \quad (2)$$

where β is the measured FWHM in radians, θ is the Bragg angle of the diffraction peak.

λ is the X-ray wavelength, L is the average particle size and ε is the effective strain. The plot of $\beta\cos\theta$ versus $\sin\theta$ for three different samples prepared at different PVA: $ZnCl_2$ ratio (5:2-5:4) and pH of the samples 1.7 is shown in Fig. 3.

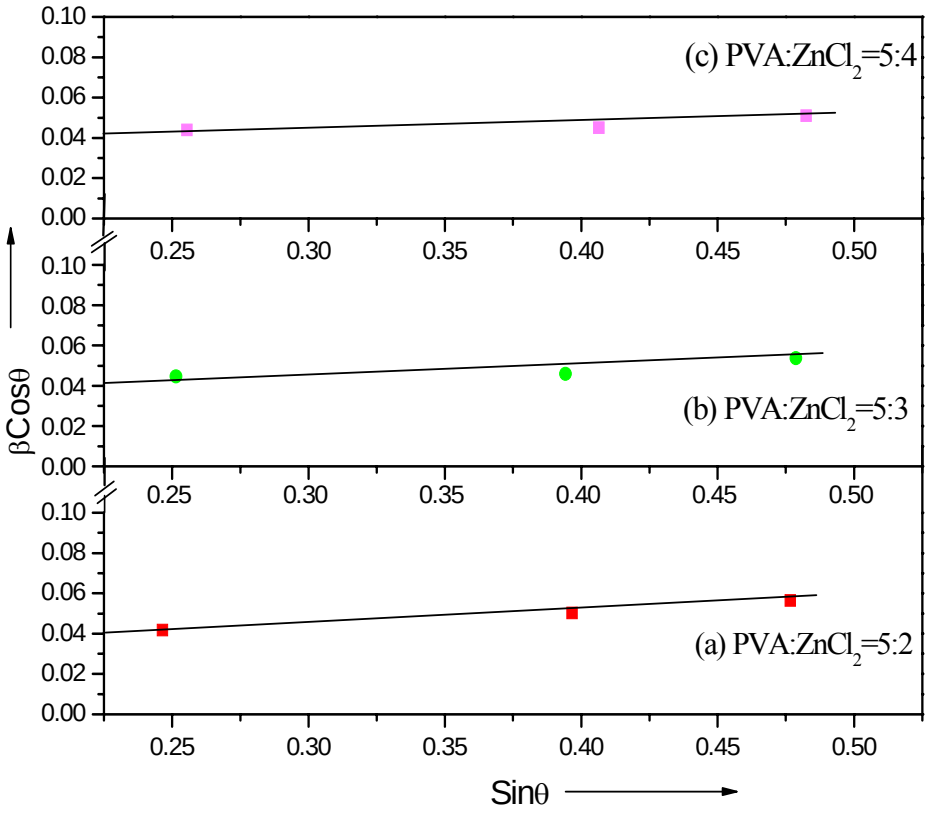

Fig. 3. Williamson-Hall plot for sample at (a) PVA: $ZnCl_2$=5:2 (b) PVA: $ZnCl_2$=5:3. (c) PVA: $ZnCl_2$=5:4.

The FWHM parameter in the above equation must be corrected with the instrumental broadening. The value of β_{inst} was determined to be 2.58×10^{-3} rad by using a standard silicon powder. However, the broadening (FWHM) observed in our sample are much higher then the instrumental broadening. Thus the major contribution to the line broadening in our sample should be arising from strain and size effect. Thus, it is clear that when $\beta\cos\theta$ is plotted against $\sin\theta$ a straight line with slope and intercept is obtained, as shown in Fig. 3 (a)-(c) From the slope of this straight line, the lattice strain and grain size for different concentration of reagent is shown in the Table 2.

Table 2. Particle size and strain at different PVA: $ZnCl_2$ concentration.

Sample	PVA:$ZnCl_2$	Strain X 10^{-3}	Crystallie size (nm)
(a)	5:1	7.2	3
(b)	5:2	6.32	4
(c)	5:3	3.4	6.8
(d)	5:4	2.63	8

It is seen from the Table that when the ratio of PVA: $ZnCl_2$ decrease (i.e. amount of $ZnCl_2$ increases) the crystallite size increases and strain decreases. The amount

of reagent ($ZnCl_2$) control the rate of reaction and hence controls the size of the particle.

Optical absorption as a function of wavelength for the PVA–ZnS composites at various $ZnCl_2$ concentrations is shown in Fig. 4.

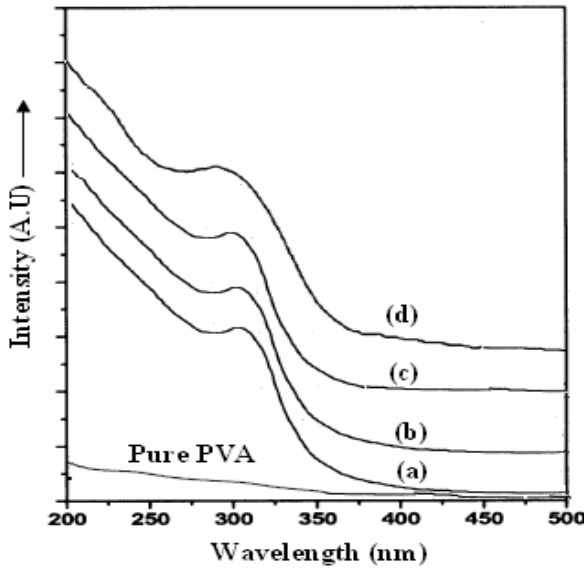

Fig. 4. UV–VIS spectra of the PVA films containing ZnS nanoparticles, preparedat different amount of $ZnCl_2$: Pure PVA; (a) 4 wt%; (b) 3 wt % ; (c) 2 wt %; (d) 1 wt %.

It was found that the pure PVA film was a kind of transparent material within the measured range. As illustrated in Fig. 4, the ZnS/PVA nanocomposite films obtained with the ratio of PVA:$ZnCl_2$ at 5:4 exhibited an absorption peak of 312 nm, which was considerably blue-shifted relative to the absorption peak of bulk ZnS (336 nm), which indicate indicates the formation of ZnS particles in the PVA matrix in the nanometer regime . With decreasing the amount of $ZnCl_2$ from 3wt% to 1wt%, the absorption peak of the obtained ZnS/PVA nanocomposite films decreased gradually from 308 to 295 nm. It was worth noting that accompanying the decrease of the optical absorption edge of the nanoparticles is shifted towards the shorter wavelength region with decrease in the concentration of $ZnCl_2$. Band-gap values were obtained from the optical absorption spectra by extrapolating the straight line plot of $(\alpha h\nu)^2$ versus $(h\nu)$ to the energy axis(not shown) . Energy band gap of the nanocrystals as given by [26]

$$E(R) = \frac{\hbar^2\pi^2}{2R^2}\left[\frac{1}{m_e^*}+\frac{1}{m_h^*}\right] - \frac{1.786e^2}{\varepsilon R} - \frac{0.124e^4}{\hbar^2\varepsilon^2}\left[\frac{1}{m_e^*}+\frac{1}{m_h^*}\right]^{-1} \quad (3)$$

where $E(R)=E_{np}- E_g$, E_{ng} is the bandgap of the ZnS nanoparticle, E_g the band gap of bulk ZnS (3.68 eV), m_e^* the effective mass of electron ($0.34m_0$), m_h^* the effective mass of hole ($0.23m_0$), r the radius of the particle, ϵ_r the dielectric constant (8.76) and ϵ_0 is the permittivity of free space. Using the above equation 3, we have estimated the particle sizes of ZnS nanoparticles in PVA matrix prepared under different concentrations of $ZnCl_2$ salt. Table 3 shows the energy band gaps and estimated particle sizes of nanoparticles. Variation in particle size with changing concentration of $ZnCl_2$ for fixed PVA concentration (5 Wt%) is shown in Fig. 5.

Table 3. Size and band gap calculation from EMA model.

Sample No.	PVA:$ZnCl_2$	Band gap (eV)	Particle size from EMA model (nm)
(a)	5:1	4.1	3.8
(b)	5:2	4.02	5
(c)	5:3	3.97	7
(d)	5:4	3.8	8.8

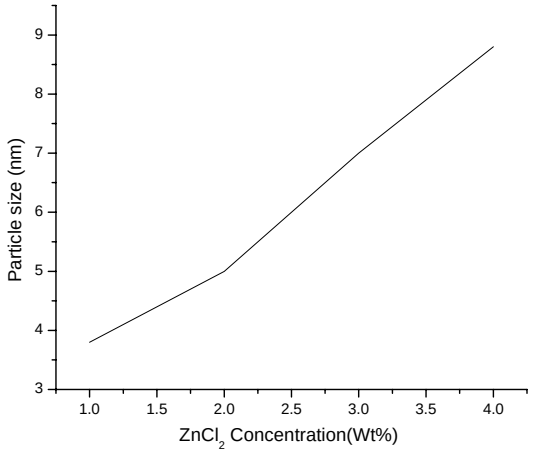

Fig. 5. Figure showing the variation of particle size function of $ZnCl_2$ concentration.

The photoluminescence (PL) spectrum of the ZnS/PVA film excited a 260 nm displays a broad emission centered at 450 nm (Fig. 6). Photoluminescence in this spectral region is attributed to the presence of sulfur vacancies in the lattice [27] This emission results from the recombination of photogenerated charge carrier in shallow traps [27]

There is a blue shift in the luminescence spectrum of ZnS nanoparticle embedded in a PVA matrix depending on the amount of $ZnCl_2$ salt, as the ratio decrease the blue shift was found to increases. Fig.6 shows the pholuminescence of ZnS nanoparticle prepared with different size. The maximum emission wavelength was found to decrease as the particle size decreased; this effect may be related to the quantum confinement effects. The larger ZnS/PVA Nanoparticle have a continuous surface with localized trapping defects relative to the core lattice, while smaller ZnS/PVA nanoparticles were found to have discontinuous surface.

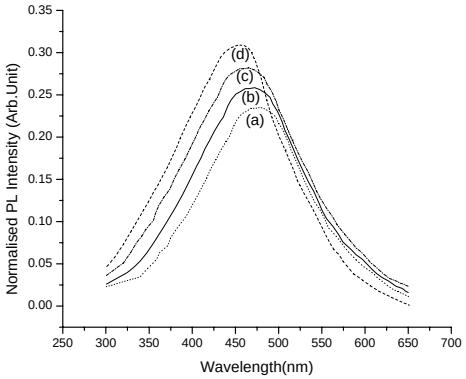

Fig. 6. Photoluminescence emission spectra for the PVA films containing ZnS nanoparticles, prepared at different amount of $ZnCl_2$ salt: (a)4 wt% (b) 3 wt% (c) 2 wt% (d) 1 wt%.

Therefore, the valence and conduction bands are replaced by more widely spaced individual energy levels in the smaller size, the lowest of which give rise to the observed luminescence [28]. The broad emission spectra observed for all nanoparticle films can be explain as follows. Photogenerated charge carriers, which have been trapped in shallow and deep surface states, tunnel to each other to recombine. Emission from recombination of short-distance pairs (in shallow traps) appears at lower wavelength than that from long distance pairs (in deep traps).Broad emission bands represent a superposition of the wide distribution of trap distance [29].

The ZnS nanoparticles may be bound by the chemical interactions between ZnS and –OH units of PVA. The interaction between Zn(S) and PVA was studied by FTIR spectra, which were used to monitor the formation of ZnS/PVA nanocomposite films. The FTIR spectra in PVA and ZnS/PVA were shown in Fig. 7.

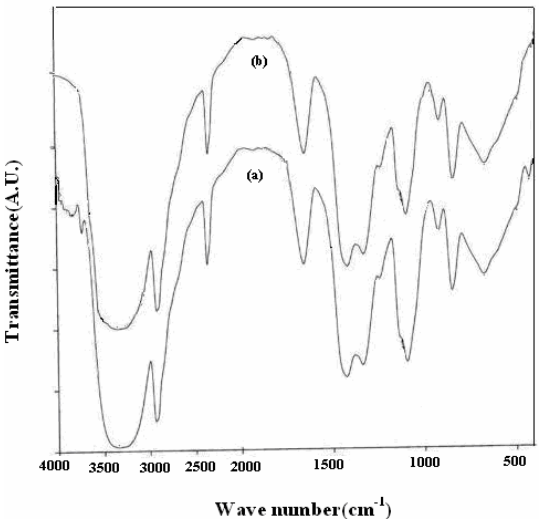

Fig. 7. FT-IR spectra of pure PVA and as-prepared PVA/ZnS composite films: (a) pure PVA film, (b) PVA/ZnS, nanocomposite (PVA:$ZnCl_2$ =5:1) film.

Two characteristic bands at 3353 and 1093 cm^{-1} were observed. The absorption band at 3353 cm^{-1} in all spectra was attributed to the O–H stretching vibration band. And another absorption band at 1093 cm^{-1} was attributed to the hydroxy C–O stretching band. Notably, compared with pure PVA, the absorption band at 3353 cm^{-1} became wide and the intensity of the absorption bands at 3353 and 1093 cm^{-1} were weaken, also the peak at 3353 cm^{-1} is shifted to 3335 cm^{-1} (see figure (curve(b)). This result indicates the interaction between –OH group and ZnS nanoparticles.The intensity of the band at 1093 cm^{-1} was also a measure of the degree of crystallinity of PVA [30]. Thus, this result clearly supported the suggestion that the introduction of ZnS decreased the degree of crystallinity of PVA, which was consistent with the XRD results.

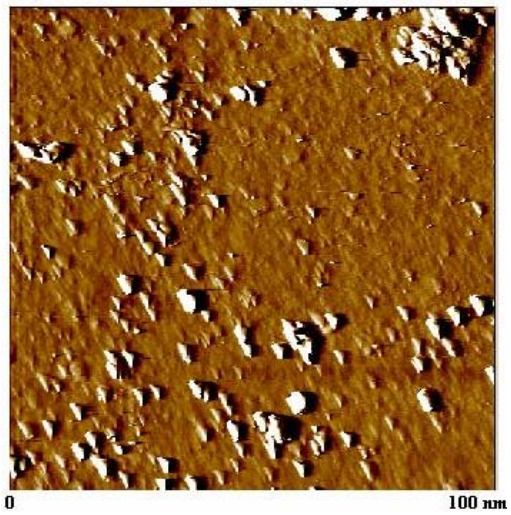

(a)

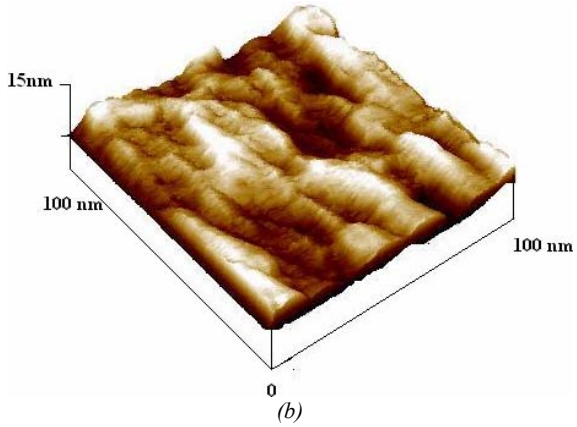

(b)

Fig. 8. (a): AFM 2D plot of ZnS nanoparticles. (PVA:$ZnCl_2$=5:2); (b) AFM 3D plot of ZnS nanoparticles.(PVA:$ZnCl_2$=5:3).

Fig. 8 (a) shows the 2D AFM image of a ZnS sample at PVA:$ZnCl_2$ ratio 5:2 of scan area 3000 nmX3000 nm. The surface appears nearly flat as observed by AFM. Fig. 8 (b) shows 3D view of another sample at PVA:$ZnCl_2$=5:3 of scan area 2000 nm X 2000 nm. The film consisted mainly of dispersed particles no larger than 8 nm in

diameter except for a few odd large ones. For all the samples, further AFM results (not shown) confirmed that the particle size in the film did increase with increasing PVA: $ZnCl_2$ ratio. With AFM color phase analysis, the two different colors in all the samples of the AFM images provide evidence that the film existed in two different phases representing, respectively, the ZnS nanoparticles and the PVA matrices Both the picture indicates that PVA:$ZnCl_2$ ratio control the surface roughness and particle size and its distribution.

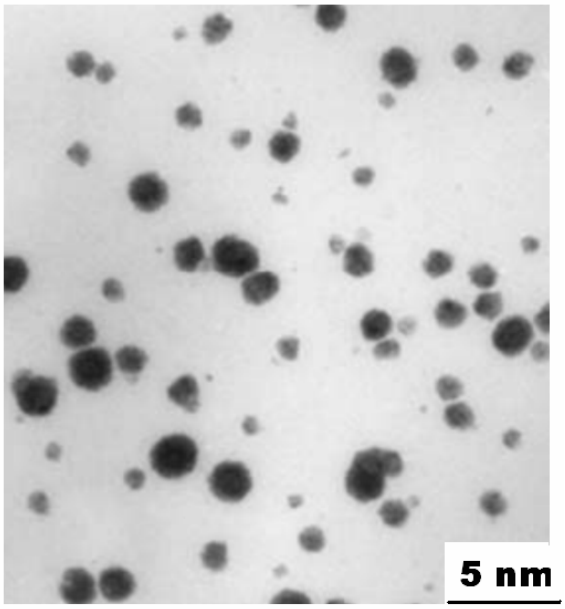

Fig. 9. TEM micrographs of the PVA films containing ZnS nanoparticles (PVA:$ZnCl_2$=5:4).

The morphologies of the nanocrystals were observed by TEM. Fig. 9 shows the overview image of the nanocrystals at PVA: $ZnCl_2$= 5:4. The particles show spherical shape and have nearly uniform size. The average particle sizes were determined from TEM micrographs and found to lie in the range of 3–12 nm, which is consistent with the UV-visible and XRD results.

Conclusions

ZnS/PVA nanocomposite films were synthesized by means of the Chemical synthesis method. XRD results indicated the Cubic phase of ZnS nanoparticles were formed within the PVA matrix. TEM image directly showed the morphology and size distribution of ZnS nanoparticles in the as-prepared ZnS/ PVA composite films. With the amount of $ZnCl_2$ salt decreasing, the size of ZnS nanoparticles in the PVA films decreased. Compared with ZnS bulk material, all the UV absorption spectra had shown explicit blue shift due to quantum confinement. FTIR spectra were used to monitor the formation of ZnS/PVA nanocomposite films. The PL emission spectrum at 450 nm is slightly blue shifted which is only due to quantum confinement effect of the nanoparticle. The as obtained AFM image shows that PVA:$ZnCl_2$ ratios control the surface roughness and particle size and the size distribution.

Acknowledgments

The authors would like to acknowledge Physics Dept and CIF, IITG for providing XRD, PL and AFM facilities. We would also like to acknowledge RSIC, NEHU Shillong for TEM observations and Department of Chemistry, Gauhati University for Spectrophotometer and FTIR observation.

References

[1] M. C. Brelle, C. L. Torres-Martinez, J. C. Mcnulty, R. K. Mehra, J. Z. Zhang, Appl. Chem. **72,** 101 (2000).
[2] C. B. Murray, D. J. Norris, M. G. Bawendi, J. Am. Chem. Soc. **115**, 8706 (1993).
[3] L. Li, J. Hu, W. Yang, A. P. Alivisatos, Nano Letters **1,** 349 (2001).
[4] G. Brusatin, M. Guglielmi, P. Innocenzi, A. Martucci, G. Scarcini, J. Electroceram. **4**, 151 (2000).
[5] P. N. Prasad, Curr. Opin. Solid State Mater. Sci. **8**, 11 (2004).
[6] M. T. Nenadovic, M. I. Comor, V. Vasic, O. I. Micic, J. Phys. Chem. **94,** 6390 (1990).
[7] S. Wang, S. Yang, Langmuir **16,** 389 (2000).
[8] Y. Wang, A. Suna, W. Mahler, R. Kasowski, J. Chem. Phys. **87**, 7315 (1987).
[9] R. S. Kane, R. E. Cohen, R. Silbey, J. Phys. Chem. **100**, 7928 (1996).
[10] J. Kuljanin, M. I. Comor, V. Djokovic, J. M. Nedeljkovic, Mater. Chem. Phys. **95,** 67 (2006).
[11] C. Falcony, M. Garcia, A. Ortiz, J. C. Alonso, J. Appl. Phys. **72**, 1525 (1992).
[12] M. Bredol, J. Merikhi, J. Mater. Sci. **33**, 471 (1998).
[13] J. Leeb, V. Gebhardt, G. Müller, D. Haarer, D. Su, M. Giersig, G. McMahon, L. Spanhel , J. Phys. Chem. B **103,** 7839 (1999).
[14] W. Chen, Z. Wang, Z. Lin, L. Lin, Appl. Phys. Lett. **70**, 1465 (1997).
[15] S. Yanagida, H. Kawakami, Y. Midori, H. Kizumoto, C. J. Pac, Y. Wada, Bull. Chem. Soc. Jpn. **68**, 1811 (1995).
[16] H. Fujiwara, H. Hosokawa, K. Murakoshi, Y. Wada, S. Yanagida, Langmuir **14**, 5154 (1998) .
[17] H. Yin, Y. Wada, T. Kitamura, S. Y. Anagida, Environ. Sci. Technol. **35**, 227 (2001).
[18] X. F. Qian, J. Yin, X. X. Guo, Y. F. Yang, Z. K. Zhu, J. Lu, J.Mater. Sci. Letter **19**, 2235 (2000).
[19] W. Sang, Y. Qian, J. Min, D. Li, L. Wang, W. Shi, L. Yinfeng, Solid State Communication **121**, 475 (2002).
[20] X. F. Qian, J. Yin, X. X. Guo, X. F. Yang, Z. K. Zhu, J. Liu, J. Mater. Sci. Lett. **19,** 2235 (2000).

[21] X. F. Qian, J. Yin, J. C. Huang, X. X. Yang, Y. F. Guo, Z. K. Zhu, Mater. Chem. Phys. **68,** 95 (2001).
[22] J. B.Nelson, D. P. Riley, Proc. phys. Soc., London, **57,** 160 (1945).
[23] K. Nanda, S. N. Sarangi, S. N. Sahu, Nano Structured Materials **10**, 1401 (1998).
[24] M. Habib Ullah, N. Kim.Chang Sikha. J. Matt. Lett **61,** 4267 (2007).
[25] G. K. Williamson, W. H. Hall., Acta Metall. **1,** 22 (1953).
[26] Y. S.Yuang, F. Y. Chen, Y. Y.Lee, C. L. Liu, J. Appl. Phys. **76**, 3041 (1994).
[27] K. Sooklal, B. S. Cullum, S. M. Angel, C. J. Murphy, J. Phys. Chem. **100,** 4551 (1996).
[28] C. Burda, S. Link, M. Mohamed, M. EI-Sayed, J. Phys. Chem. B **105**, 12286 (2001).
[29] I. Spanbel, M. A. Anderson, J. Am. Chem. Soc., 2826 (1991).
[30] S. Krimm, C. Y. Liang, G. B. B. M. Sutherland, J. Polym. Sci. **XXII**, 227 (1956).

*Corresponding author: jpb@iitg.ernet.in